Observer repeatability and interscan reproducibility of 18F-sodium fluoride coronary microcalcification activity

Evangelos Tzolos* [a, b] Jacek Kwiecinski* [a, c], Martin Lyngby Lassen [a], Sebastien Cadet [a], Philip D Adamson [b, d], Alastair J Moss [b, e], Nikhil Joshi [b, e], Michelle C Williams [b, f], Edwin JR van Beek [b, f], Damini Dey [a], Daniel S Berman [a], Marc R Dweck [b], David E Newby [b, e], Piotr J Slomka [a]

a Department of Imaging (Division of Nuclear Medicine), Medicine, and Biomedical Sciences, Cedars-Sinai Medical Center, Los Angeles, CA, USA

b BHF Centre for Cardiovascular Science, University of Edinburgh, Edinburgh, United Kingdom

c Department of Interventional Cardiology and Angiology, Institute of Cardiology, Warsaw, Poland

d Christchurch Heart Institute, University of Otago, Christchurch, New Zealand

e BHF Cardiovascular Research Centre, University of Leicester, Leicester, United Kingdom

f Edinburgh Imaging, Queens Medical Research Institute, University of Edinburgh, Edinburgh, United Kingdom

*equal contribution as first author

Address for Correspondence:

Piotr J. Slomka, PhD

Artificial Intelligence in Medicine Program

Cedars-Sinai Medical Center

8700 Beverly Blvd, Ste A047N

Los Angeles, CA 90048, USA

Email: piotr.slomka@cshs.org

Phone: 310-423-4348   Fax: 310-423-0173

Funding

Abstract

Background (words 199/200)

We aimed to establish the observer repeatability and interscan reproducibility of coronary ^{18}F-sodium fluoride (^{18}F-NaF) positron emission tomography (PET) uptake using a novel semi-automated approach, coronary microcalcification activity (CMA).

Methods

Patients with multivessel coronary artery disease underwent repeated hybrid PET and computed tomography angiography (CTA) imaging (PET/CTA). CMA was defined as the integrated standardized uptake values (SUV) in the entire coronary tree exceeding 2 standard deviations above the background SUV. Coefficients of repeatability between the same observer (intraobserver repeatability), between 2 observers (interobserver repeatability) and coefficient of reproducibility between 2 scans (interscan reproducibility), were determined at both vessel and patient level.

Results

In 19 patients, CMA was assessed twice in 43 coronary vessels on two PET/CT scans performed 12±5 days apart. There was excellent intraclass correlation on a per-vessel and per-patient level for intraobserver and interobserver repeatability as well as interscan reproducibility (≥0.991 for all). There was 100% intraobserver, interobserver and interscan agreement for the presence (CMA>0) or absence (CMA=0) of coronary ^{18}F-NaF uptake. Mean CMA was 3.12±0.62 with coefficients of repeatability of ≤10% for all measures: intraobserver 0.24 and 0.22, interobserver 0.30 and 0.29 and interscan 0.33 and 0.32 at a per-vessel and per-patient level respectively.

Conclusions

CMA is a repeatable and reproducible global measure of coronary atherosclerotic activity.

Abbreviations

CMA	coronary microcalcification activity
[18]F-NaF	^{18}F-sodium fluoride
PET	positron emission tomography
CTA	computed tomography angiography
MC	cardiac motion corrected
BC	background blood pool clearance correction
TBR	target to background ratio
SUV	standardized uptake value
TBR$_{MAX}$	maximum target to background ratio
SUV$_{MAX}$	maximum standardized uptake value
VOI	volume of interest
BMI	body-mass index

Introduction

Hybrid positron emission tomography and computed tomography (PET/CT) imaging with ^{18}F-sodium fluoride (^{18}F-NaF) can be used as a marker of developing microcalcification across multiple different vascular and valvular disease states (1-6). It has been used to assess atherosclerotic disease activity in the coronary arteries, with the potential to identify high-risk plaques (1, 7-10). To date, most studies have reported coronary ^{18}F-NaF PET uptake using maximum target to background ratio (TBR$_{MAX}$) (3, 7, 9, 11, 12). While TBR$_{MAX}$ has been used as the primary measure for individual lesions (11, 13), its measurement can vary depending on plaque activity, the anatomical location of the background activity measured, and the partial volume effects of such small structures (14, 15).

We have developed a novel semi-automated approach to measure ^{18}F-NaF uptake throughout the entire coronary vasculature. This method uses centerlines defined by coronary CT angiography to build 3-dimensional tubular volumes of interest around each of the main epicardial coronary arteries (8) and thereby derive a single summary measure of total coronary microcalcification activity (CMA). This method allows evaluation of coronary ^{18}F-NaF activity on a per-vessel and per-patient basis, providing a global assessment of disease activity in the coronary arteries that is akin to the Agatston coronary artery calcium score for CT-defined coronary macrocalcification (8). CMA appears to correlate more closely with established CT-derived markers of plaque vulnerability than TBRmax (9). However, the observer repeatability and interscan reproducibility of CMA has yet to be established. In this study, we aimed to evaluate the intra- and interobserver repeatability and interscan reproducibility of CMA.

Materials and Methods

Study Population

Twenty patients underwent two ^{18}F-NaF PET/CT examinations of the coronary arteries within three weeks of each other as a part of the DIAMOND (Dual antiplatelet therapy to inhibit Atherosclerosis and Myocardial injury in patients with Necrotic high-risk coronary plaque Disease , NCT02110303) study (16). Inclusion in the study required angiographically confirmed multivessel coronary artery disease, defined by either previous revascularization or stenosis >50% in at least two major epicardial coronary arteries. Exclusion criteria were an acute coronary syndrome within 12 months prior to the examination, renal dysfunction (estimated glomerular filtration rate ≤30 mL/min/1.73 m^2) and contraindication to iodinated contrast media. This study was approved by the Scottish research ethics committee (REC reference: 14/SS/0089) and written informed consent was obtained from all participants.

Image Acquisition Protocol (PET/CT acquisition)

All patients underwent two ^{18}F-NaF PET/CT scans within three weeks.

PET acquisition

Patients underwent a 30-min list-mode PET-emission acquisitions approximately 1 h after injection of 250 MBq of ^{18}F-NaF. All patients were scanned with arms positioned above the head in a 128-slice Biograph mCT system (Siemens Healthineers, Knoxville, TN, USA). A low-dose CT for attenuation correction was acquired immediately before the PET acquisition (120 kV, 50 mAs, 3-mm slice thickness). All patients were imaged with 3-lead electrocardiogram cardiac gating.

CCTA acquisition

For anatomical localization of PET uptake, coronary computed tomography angiography (CCTA) was performed immediately after the PET acquisition. The CCTA was performed using prospective gating, 330 ms rotation time, body-mass index (BMI) dependent voltage (<25 kg/m^2, 100 kV; ≥25 kg/m^2, 120 kV), and tube-current time product of 160–245 mAs. Patients were administered oral or intravenous beta-blocker therapy to achieve a target heartrate of <60 beats/min. A BMI-dependent bolus-injection of contrast media (400 mg/mL) was administered to the patients with a flow of 5–6 mL/s after determining the appropriate trigger delay defined by a test bolus of 20 mL of contrast material.

Image Analysis Protocol

PET reconstruction

PET images were reconstructed into 4 cardiac phases using a vendor provided software (JS-Recon12, Siemens, Knoxville, TN, USA). All PET image reconstructions were performed with corrections for time-of-flight and point-spread function. Using 4 cardiac gates, we reconstructed the data on a 256 × 256 matrix (109 slices, slice thickness 2.027 mm) using 2 iterations, 21 subsets and 5-mm Gausian filter.

Cardiac Motion correction

Cardiac motion corrected images were obtained from the gated PET reconstructions through PET-PET image co-registration using a diffeomorphic registration and dedicated software (FusionQuant version 1.19.2.7, Cedars-Sinai Medical center) (17).

Image registration

Prior to image analysis, the PET reconstructions were registered to the CCTA images, using a rigid translation of the PET images. The PET to CCTA registration was ensured using five key points of reference; sternum, vertebrae, blood pool in the left and right ventricle (based upon high ^{18}F-NaF activity in the blood pool in comparison to the surrounding myocardium), and the great vessels (18).

Blood clearance correction

To minimize the impact of variations in background blood pool activity introduced by the injection-to-scan delays (13, 19), we standardized the background blood pool activity to an injection-to-scan delay of 60 minutes using a previously described correction factor (13) (Eq. 1)

SUVBackground corrected = SUVBackground*e(−0.004*(60−t))   (1)

where t represents the injection-to-scan delay in minutes.

CMA quantification

Based upon PET image analysis techniques widely used in oncology and cardiac sarcoidosis (20-22) as well as the Agatston method for quantifying coronary CT calcium scores, we developed a novel measure to assess whole vessel activity in the coronary tree (8). To obtain the CMA values, two distinct steps were performed. First, we selected the proximal and distal end of the vessel (>2 mm) and applied a vessel tracking algorithm to extract whole-vessel tubular 3D volumes of interest from CCTA using dedicated semi-automated Autoplaque software (version 2, Cedars-Sinai Medical

Center, Los Angeles, CA)(23) (Figure 1). These encompass all the main epicardial coronary vessels and their immediate surroundings (4-mm radius) facilitating per-vessel and per-patient uptake quantification. In a tubular VOI, along the extracted centerlines, with 4-mm radius, we measured the CMA on the PET/CCTA co-registered images. For this study, we evaluated ^{18}F-NaF activity along the entire course of coronary arteries regardless of the presence of coronary stents, and we included the left main in the left anterior descending artery VOI. CMA was defined as the average SUV within the activity volume above threshold of background SUV mean +2 standard deviations. The background activity was measured in the right atrium.

TBR$_{MAX}$ quantification

CTA studies were assessed visually for percent stenosis according to the Society of Cardiovascular Computed Tomography guidelines (24). For a signal to be co-localized to a coronary artery, an atherosclerotic plaque had to be present on CT angiography, and the increased pattern of radiotracer had to arise from the coronary artery and follow its course over >5 mm in three dimensions on orthogonal views (25). On the co-registered PET and CTA images, ^{18}F-NaF PET uptake was measured in all coronary segments with a vessel diameter ≥2 mm and >25% stenosis as defined by CTA. The ^{18}F-NaF uptake in these lesions was evaluated in a 3D spherical volume of interest (VOI) (radius 5 mm). In all plaques meeting these criteria, the maximum standardized uptake values (SUV$_{MAX}$) were measured within manually drawn regions of interest. TBR$_{MAX}$ values were calculated by dividing the coronary SUV$_{MAX}$ by the blood pool activity measured in the right atrium (cylindrical volume of interest radius 10 mm and thickness 5 mm) at the level of the right coronary artery ostium.

Diagnostic Evaluation of CMA and TBR$_{MAX}$

Using CMA, the individual coronary arteries were marked as ^{18}F-NaF positive if CMA>0 and negative if CMA =0 (8). We also assessed the burden of activity on a per-vessel and per-patient level. To allow a per-patient analysis, we added the CMA activity of all major epicardial vessels (CMA$_{total}$). For TBR, PET uptake was quantified based on the CCTA lesion position, with lesions categorized as ^{18}F-NaF-positive (TBR$_{MAX}$ ≥1.25) or ^{18}F-NaF-negative (TBR$_{MAX}$ <1.25) (3, 7, 26). In order to compare TBR$_{MAX}$ with CMA, we plotted the percentage differences in Bland-Altman plots.

Observer Repeatability and Interscan Reproducibility

Two anonymized scans for each of the 20 patients were presented to 2 experienced observers in random order. First, repeat assessments (observations 1 & 2) were performed by observer 1 at least 12 weeks apart in random order to prevent recall bias (intraobserver repeatability). Secondly, a second observer (observer 2) perfomed analysis for both scans and we compared them with measurements performed by the first obsrever (interobserver repeatability). Lastly, we compared the measurements between baseline scan (scan1) and repeat scan 2-3 weeks later (scan 2) in order to compute the interscan reproducibility.

Statistical analysis

Data were tested for normality using the Shapiro–Wilk test. Statistical analysis was performed using MedCalc Statistical Software version 16.4.3 (MedCalc Software bv, Ostend, Belgium). Continuous, normally distributed variables were presented as mean ±

standard deviation, whereas non-normally distributed continuous data were presented as median [range]. Assessment of CMA and TBR$_{MAX}$, observer repeatability and interscan reproducibility were obtained using descriptive statistics with intraclass correlation coefficient (ICC) as well as Bland–Altman plots with mean bias and limits of agreement (LOA).

Results

Twenty patients were recruited (Table 1), although one patient was excluded from the study due to incomplete list mode PET data. From the 57 coronary arteries included in the study, a total of 49 vessels fitted the size criterion (>2 mm in diameter). We excluded 6 vessels from the analysis: all vessels were the left circumflex coronary artery and were excluded due to spillover of ^{18}F-NaF activity from neighboring mitral valve calcification (3 from scan 1 and 3 from scan 2), leaving a total of 43 vessels for the final analysis. A total of 47 lesions were identified on CCTA in these 43 vessels. The mean uptake values observed for the two readers and the repeated scans were 3.12± 0.62 for CMA and 1.62±0.49 for TBR$_{MAX}$.

Presence or absence of ^{18}F-NaF activity

There was 100% intraobserver, interobserver and interscan agreement for the presence of ^{18}F-NaF activity (CMA>0) or absence of ^{18}F-NaF activity (CMA=0) (Table 2). In addition, there were excellent intraclass correlations between the same observer, different observers and between scans (Table 3).

Intraobserver analysis

There was excellent intraobserver repeatability for CMA measurement on a per-vessel level, with a coefficient of repeatability of 0.24, mean bias of −0.02 (p=0.39) and narrow limits of agreement (95% LOA −0.25 to 0.22; Figure 2A). Similarly, at a patient level, CMA$_{total}$ repeatability coefficient was 0.22 with a mean bias of −0.03 (p=0.12) and narrow limits of agreement (95% LOA −0.25 to 0.18; Figure 2B).

Interobserver analysis

Comparable to the intraobserver analysis, there was also excellent interobserver repeatability for CMA measurement on a per-vessel level, with a coefficient of repeatability of 0.30, mean bias of −0.01 (p=0.79) and narrow limits of agreement (95% LOA −0.31 to 0.29; Figure 3A). At a patient level, CMA$_{total}$ repeatability coefficient was 0.29 with a mean bias of −0.04 (p=0.17) and narrow limits of agreement (95% LOA −0.33 to 0.25; Figure 3B).

Interscan analysis

Similar to the interobserver analysis, interscan analysis of CMA showed very good reproducibility. At a vessel level, there was excellent interscan reproducibility with a coefficient of reproducibility of 0.33, mean bias of 0.02 (p=0.89) and narrow limits of agreement (95% LOA −0.31 to 0.35; Figure 4A). Likewise, at a patient level, CMA$_{total}$ reproducibility coefficient was 0.32 with a mean bias of −0.02 (p=0.30) and narrow limits of agreement (95% LOA −0.34 to 0.28; Figure 4B).

CMA and TRB$_{MAX}$

The activity of separate lesions (n=47) was assessed using maximum target-to-background ratio (TBR$_{MAX}$. Compared to TBR$_{MAX}$, CMA showed superior limits of agreement and smaller coefficients of repeatability for intraobserver, interobserver and , coefficient or reproducibility interscan analyses. Between the same observer, CMA showed a mean bias and limits of agreement of 0.2% (95% LOA -10.6 to 11.1%) and TBR$_{MAX}$ showed a bias of -2.4% (95% LOA -20.7 to 15.9%) with coefficients of repeatability of 10.8% and 18.3% respectively (Supplement Figure 1). Similarly,

between different observers, CMA was more reproducible than TBR_{MAX} with a mean

bias and limits of agreement of -0.1% (95% LOA -14.1 to 4.0) and -3.75% (95% LOA -

25.2% to 17.8%) respectively and coefficients of repeatability of 14.0% and 19.5%

(Supplement Figure 2). Finally, between scans, CMA showed a mean bias and limits of

agreement of 0.1% (95% LOA -17.4 to 17.2%) and TBR_{MAX} showed a bias of 0.3%

(95% LOA -24.0% to 24.6%) with coefficients of reproducibility of 17.2% and 24.3%

respectively (Supplement Figure 3).

Discussion

Coronary ^{18}F-NaF PET is a non-invasive tool for imaging vulnerable atherosclerotic

plaques (7, 8). We evaluated the repeatability and reproducibility of a novel

methodology (CMA) for assessing whole vessel coronary ^{18}F-NaF uptake on PET/CT as

a single measure of patient risk (8). We showed that CMA has excellent intra- and

interobserver repeatability and interscan reproducibility and narrow limits of agreements

within and between scans. This suggests that CMA is sufficiently robust to be used as

single measure of coronary atherosclerotic activity and has the potential to provide a

summary score of coronary risk similar to that described by the Agatston coronary

artery calcium score (27).

It is now widely accepted that the anatomic assessment of the whole-coronary disease

burden (vulnerable patient) is of greater importance than the identification of a single

vulnerable plaque (28-30). We have shown that both TBR$_{MAX}$ and CMA assessments

were repeatable and reproducible, albeit CMA had the best repeatability and

reproducibility. This has important implications for serial scanning and monitoring

disease progression with coronary PET. Furthermore, there was no diagnostic

discordance between observers or scans for CMA, something that is not always true for

TBR$_{MAX}$. For the presence or absence of CMA, there was 100% agreement in the

categorization between observers or scans with no crossover of cases observed. On

the other hand, there were 3 discordant values for TBR$_{MAX}$ between observers and 4

discordant values between scans.

This is the first study investigating the repeatability and interscan reproducibility of both

CMA and TBR$_{MAX}$. In a previous study (11), we showed that TBR$_{MAX}$ displayed good

observer repeatability and interscan reproducibility when employing mid-diastolic PET images. This can be further improved using cardiac motion-corrected reconstructions (13). However, we have here reported narrower limits of agreement for observer repeatability and interscan reproducibility, both at a vessel as well as at a patient level.

Another strength of CMA is that it integrates the total activity of all 3 vessels in a score that resembles the well-established calcium score i.e. a patient with CMA= 0 has no active microcalcification similar to a patient with zero calcium score. CMA moves away from a single hot-spot approach to a patient-level total ^{18}F-NaF activity burden assessment and hence does not rely on a single pixel-value leading to better reproducibility. Furthermore, by identifying the coronary artery borders from CTA and limiting the assessment of ^{18}F-NaF uptake within these borders, the CMA approach has the strength to reduce the subjectivity and the time required to perform image analysis.

Despite the broad application of the individual lesion assessments using TBR$_{MAX}$ (3, 7, 9, 11-13, 25, 30), this technique can only provide an estimation of activity at an individual plaque level, and as a result, the overall coronary disease burden of active macrocalcification cannot be appreciated. Indeed, this approach bears the risk of underestimating the ^{18}F-NaF activity in patients with multiple plaques with increased tracer activity across the coronary tree (Figure 5). Using CMA, and computing the total activity burden, we were able to translate ^{18}F-NaF PET tracer uptake into the total coronary macrocalcification activity mirroring an approach successfully applied in the field of oncology and cardiac sarcoidosis (metabolic activity volume) (20-22). Thus, CMA provides a measure of the overall burden of disease activity for the patient.

Finally, despite the excellent prognostic information that coronary calcium scoring provides in asymptomatic individuals (31, 32) and those presenting with chest pain (33), its prognostic capability has been suboptimal in studies involving patients with established advanced coronary artery disease (34, 35). While coronary calcium visualizes advanced and potentially healed disease (macrocalcification), it lacks the ability to visualize active disease (microcalcification) or predict future calcification progression. On the other hand, ^{18}F-NaF uptake is associated with culprit coronary plaques in patients with myocardial infarction (7), adverse plaque features in patients with apparently stable disease (9) and predicts the future progression of coronary calcium scores, confirming its status as a marker of disease activity (36). In addition, in a small study involving 32 patients, Kitagawa et al (12) showed that higher ^{18}F-NaF uptake in established coronary atherosclerotic lesions on PET has a predictive value for future cardiac events (acute coronary syndrome or late coronary revascularization) that was superior to the predictive value of the findings on CCTA, including coronary artery stenosis, high risk plaques and calcification. Moreover our group has recently shown, in a large multicohort study involving 293 patients with established multivessel coronary artery disease, that CMA outperforms coronary calcium score in prediction of myocardial infarction and major adverse acardiovascualr events (MACE) (37, 38).

Limitations

This study has several additional limitations; first is the number of patients included in the study (19). Despite the low number of participants, we were able to identify 47 separate lesions and we have evaluated each patient both at a per-vessel level and per-patient level. Another limitation was that we used only cardiac motion corrected images and did

not apply gross patient motion and respiratory motion corrections (triple motion corrections)(13). The third limitation of this study was that all lesions were manually delineated by only two expert readers which may affect its broader generalisability. Finally, this study was obtained in a single center using a PET/CT system from one vendor only. A bigger multicenter study including systems from multiple vendors would be required to confirm our findings.

New Knowledge Gained

Using CMA provides an accurate and highly reproducible metric of ^{18F}-NaF PET/CT uptake. This finding is important to ensure the optimal quantitative accuracy in studies utilizing ^{18}F-NaF, such as PREFFIR [NCT02278211](11), a study involving 700 patients with multi-vessel coronary artery disease. Based on this finding and given the comparable reproducibility of TBR$_{MAX}$, both approaches can be implemented in future clinical trials.

Conclusion

In conclusion, we have shown CMA provides a novel metric of the per-vessel and per-patient coronary ^{18}F-NaF PET activity that has excellent intraobserver, and interobserver repeatability and interscan reproducibility. We suggest that CMA could be used as a global patient level measure of ^{18}F-NaF uptake with potential application to clinical trials and clinical practice.

References

(1)   Irkle A, Vesey AT, Lewis DY, Skepper JN, Bird JL, Dweck MR et al. Identifying active vascular microcalcification by (18)F-sodium fluoride positron emission tomography. Nat Commun 2015;6:7495.

(2)   Creager MD, Hohl T, Hutcheson JD, Moss AJ, Schlotter F, Blaser MC et al. (18)F-Fluoride Signal Amplification Identifies Microcalcifications Associated With Atherosclerotic Plaque Instability in Positron Emission Tomography/Computed Tomography Images. Circ Cardiovasc Imaging 2019;12:e007835.

(3)   Dweck MR, Chow MW, Joshi NV, Williams MC, Jones C, Fletcher AM et al. Coronary arterial 18F-sodium fluoride uptake: a novel marker of plaque biology. J Am Coll Cardiol 2012;59:1539-48.

(4)   Dweck MR, Jenkins WS, Vesey AT, Pringle MA, Chin CW, Malley TS et al. 18F-sodium fluoride uptake is a marker of active calcification and disease progression in patients with aortic stenosis. Circ Cardiovasc Imaging 2014;7:371-8.

(5)   Massera D, Trivieri MG, Andrews JPM, Sartori S, Abgral R, Chapman AR et al. Disease Activity in Mitral Annular Calcification. Circ Cardiovasc Imaging 2019;12:e008513.

(6)   Cartlidge TRG, Doris MK, Sellers SL, Pawade TA, White AC, Pessotto R et al. Detection and Prediction of Bioprosthetic Aortic Valve Degeneration. J Am Coll Cardiol 2019;73:1107-19.

(7)   Joshi NV, Vesey AT, Williams MC, Shah AS, Calvert PA, Craighead FH et al. 18F-fluoride positron emission tomography for identification of ruptured and high-risk coronary atherosclerotic plaques: a prospective clinical trial. Lancet 2014;383:705-13.

(8)   Kwiecinski J, Cadet S, Daghem M, Lassen ML, Dey D, Dweck MR et al. Whole-vessel coronary (18)F-sodium fluoride PET for assessment of the global coronary microcalcification burden. Eur J Nucl Med Mol Imaging 2020.

(9)   Kwiecinski J, Dey D, Cadet S, Lee SE, Tamarappoo B, Otaki Y et al. Predictors of 18F-sodium fluoride uptake in patients with stable coronary artery disease and adverse plaque features on computed tomography angiography. Eur Heart J Cardiovasc Imaging 2019.

(10)   Kwiecinski J, Slomka PJ, Dweck MR, Newby DE, Berman DS. Vulnerable plaque imaging using 18F-sodium fluoride positron emission tomography. The British Journal of Radiology 2019:20190797.

(11)   Moss AJ, Doris MK, Andrews JPM, Bing R, Daghem M, van Beek EJR et al. Molecular Coronary Plaque Imaging Using (18)F-Fluoride. Circ Cardiovasc Imaging 2019;12:e008574.

(12)   Kitagawa T, Yamamoto H, Nakamoto Y, Sasaki K, Toshimitsu S, Tatsugami F et al. Predictive Value of (18)F-Sodium Fluoride Positron Emission Tomography in Detecting High-Risk Coronary Artery Disease in Combination With Computed Tomography. J Am Heart Assoc 2018;7:e010224.

(13)   Lassen ML, Kwiecinski J, Dey D, Cadet S, Germano G, Berman DS et al. Triple-gated motion and blood pool clearance corrections improve reproducibility of coronary (18)F-NaF PET. Eur J Nucl Med Mol Imaging 2019;46:2610-20.

(14)   Chen W, Dilsizian V. PET assessment of vascular inflammation and atherosclerotic plaques: SUV or TBR? J Nucl Med 2015;56:503-4.

(15)   Blomberg BA, Bashyam A, Ramachandran A, Gholami S, Houshmand S, Salavati A et al. Quantifying [18F]fluorodeoxyglucose uptake in the arterial wall: the effects of dual time-point imaging and partial volume effect correction. European Journal of Nuclear Medicine and Molecular Imaging 2015;42:1414-22.

(16)   Moss AJ, Dweck MR, Doris MK, Andrews JPM, Bing R, Forsythe RO et al. Ticagrelor to Reduce Myocardial Injury in Patients With High-Risk Coronary Artery Plaque. JACC Cardiovasc Imaging 2019.

(17)   Rubeaux M, Joshi NV, Dweck MR, Fletcher A, Motwani M, Thomson LE et al. Motion Correction of 18F-NaF PET for Imaging Coronary Atherosclerotic Plaques. J Nucl Med 2016;57:54-9.

(18)   Kwiecinski J, Adamson PD, Lassen ML, Doris MK, Moss AJ, Cadet S et al. Feasibility of Coronary (18)F-Sodium Fluoride Positron-Emission Tomography Assessment With the Utilization of Previously Acquired Computed Tomography Angiography. Circ Cardiovasc Imaging 2018;11:e008325.

(19)   Kwiecinski J, Berman DS, Lee SE, Dey D, Cadet S, Lassen ML et al. Three-Hour Delayed Imaging Improves Assessment of Coronary (18)F-Sodium Fluoride PET. J Nucl Med 2019;60:530-5.

(20)   Rahim MK, Kim SE, So H, Kim HJ, Cheon GJ, Lee ES et al. Recent Trends in PET Image Interpretations Using Volumetric and Texture-based Quantification Methods in Nuclear Oncology. Nucl Med Mol Imaging 2014;48:1-15.

(21)   Larson SM, Erdi Y, Akhurst T, Mazumdar M, Macapinlac HA, Finn RD et al. Tumor Treatment Response Based on Visual and Quantitative Changes in Global Tumor Glycolysis Using PET-FDG Imaging. The Visual Response Score and the Change in Total Lesion Glycolysis. Clin Positron Imaging 1999;2:159-71.

(22)   Ahmadian A, Brogan A, Berman J, Sverdlov AL, Mercier G, Mazzini M et al. Quantitative interpretation of FDG PET/CT with myocardial perfusion imaging increases diagnostic information in the evaluation of cardiac sarcoidosis. J Nucl Cardiol 2014;21:925-39.

(23)   Dey D, Schepis T, Marwan M, Slomka PJ, Berman DS, Achenbach S. Automated Three-dimensional Quantification of Non-calcified Coronary Plaque from Coronary CT Angiography: comparison with Intravascular Ultrasound Radiology 2010;257:516-22.

(24)   Leipsic J, Abbara S, Achenbach S, Cury R, Earls JP, Mancini GJ et al. SCCT guidelines for the interpretation and reporting of coronary CT angiography: a report of the Society of Cardiovascular Computed Tomography Guidelines Committee. J Cardiovasc Comput Tomogr 2014;8:342-58.

(25)   Doris MK, Otaki Y, Krishnan SK, Kwiecinski J, Rubeaux M, Alessio A et al. Optimization of reconstruction and quantification of motion-corrected coronary PET-CT. J Nucl Cardiol 2018.

(26)   Lassen ML, Kwiecinski J, Cadet S, Dey D, Wang C, Dweck MR et al. Data-Driven Gross Patient Motion Detection and Compensation: Implications for Coronary (18)F-NaF PET Imaging. J Nucl Med 2019;60:830-6.

(27)   Agatston AS, Janowitz WR, Hildner FJ, Zusmer NR, Viamonte M, Jr., Detrano R. Quantification of coronary artery calcium using ultrafast computed tomography. J Am Coll Cardiol 1990;15:827-32.

(28)   Arbab-Zadeh A, Fuster V. The Myth of the "Vulnerable Plaque". Transitioning From a Focus on Individual Lesions to Atherosclerotic Disease Burden for Coronary Artery Disease Risk Assessment 2015;65:846-55.

(29)   Arbab-Zadeh A, Fuster V. From Detecting the Vulnerable Plaque to Managing the Vulnerable Patient: JACC State-of-the-Art Review. J Am Coll Cardiol 2019;74:1582-93.

(30)   Bellinge JW, Francis RJ, Majeed K, Watts GF, Schultz CJ. In search of the vulnerable patient or the vulnerable plaque: (18)F-sodium fluoride positron emission tomography for cardiovascular risk stratification. J Nucl Cardiol 2018;25:1774-83.

(31)   Budoff MJ, Young R, Burke G, Jeffrey Carr J, Detrano RC, Folsom AR et al. Ten-year association of coronary artery calcium with atherosclerotic cardiovascular disease (ASCVD) events: the multi-ethnic study of atherosclerosis (MESA). Eur Heart J 2018;39:2401-8.

(32)   Greenland P, Blaha MJ, Budoff MJ, Erbel R, Watson KE. Coronary Calcium Score and Cardiovascular Risk. J Am Coll Cardiol 2018;72:434-47.

(33)   Greenland P, Bonow RO, Brundage BH, Budoff MJ, Eisenberg MJ, Grundy SM et al. ACCF/AHA 2007 clinical expert consensus document on coronary artery calcium scoring by computed

tomography in global cardiovascular risk assessment and in evaluation of patients with chest pain: a report of the American College of Cardiology Foundation Clinical Expert Consensus Task Force (ACCF/AHA Writing Committee to Update the 2000 Expert Consensus Document on Electron Beam Computed Tomography) developed in collaboration with the Society of Atherosclerosis Imaging and Prevention and the Society of Cardiovascular Computed Tomography. J Am Coll Cardiol 2007;49:378-402.

(34)   Budoff MJ, Mayrhofer T, Ferencik M, Bittner D, Lee KL, Lu MT et al. Prognostic value of coronary artery calcium in the PROMISE study (Prospective Multicenter Imaging Study for Evaluation of Chest Pain). Circulation 2017;136:1993-2005.

(35)   Erbel R, Mohlenkamp S, Moebus S, Schmermund A, Lehmann N, Stang A et al. Coronary risk stratification, discrimination, and reclassification improvement based on quantification of subclinical coronary atherosclerosis: the Heinz Nixdorf Recall study. J Am Coll Cardiol 2010;56:1397-406.

(36)   Doris M, Moss AJ, Andrews JPM, Williams M, Van Beek EJR, Forsyth L et al. Coronary 18F-sodium fluoride uptake predicts progression of coronary arterial calcification. European Heart Journal 2019;40:53-.

(37)   Kwiecinski J TE, Cadet S, Adamson PD, Moss A, Joshi NV et al. 18F-SODIUM FLUORIDE CORONARY UPTAKE PREDICTS MYOCARDIAL INFARCTIONS IN PATIENTS WITH KNOWN CORONARY ARTERY DISEASE. J Am Coll Cardiol. 2020 Mar, 75 (11 Supplement 1) 3667.; 2020.

(38)   Kwiecinski J* TE, Adamson PD, Cadet S, Moss AJ, Joshi N et al. 18F-Sodium Fluoride Coronary Uptake Predicts Outcome in Patients with Coronary Artery Disease. JACC(in press); 2020.

TABLES

Table 1

Baseline characteristics

Age (years)	70 ± 8
Gender (males)	16 (84)
Body-mass index (kg/m^2)	27.6 ± 4.0
Cardiovascular risk factors	
- Diabetes mellitus (type II)	2 (11)
- Current smoker	2 (11)
- Hypertension	13 (68)
- Hyperlipidemia	19 (100)
Agatson Calcium Score (AU)	1075 [0-1890]

Continuous variables reported as mean ± SD or median and

interquartile range [IQR]; categorical variables reported as n (%),

Table 2

Intraobserver (A), interobserver (B) and interscan (C) variability for the presence or the absence of ^{18}F-sodium fluoride uptake (coronary microcalcification activity) at a vessel level (n=43).

		Observation* 2			Observation* 2	
A **Observervation 1**		CMA>0	CMA=0		TBR$_{MAX}$≥1.25	TBR$_{MAX}$<1.25
	CMA>0	34	0	TBR$_{MAX}$≥1.25	35	2
	CMA=0	0	9	TBR$_{MAX}$<1.25	1	12
B **Observer 1**		Observer 2			Observer 2	
	CMA>0	34	0	TBR$_{MAX}$≥1.25	35	1
	CMA=0	0	9	TBR$_{MAX}$<1.25	2	12
C **Scan 1**		Scan 2			Scan 2	
	CMA>0	34	0	TBR$_{MAX}$≥1.25	34	2
	CMA=0	0	9	TBR$_{MAX}$<1.25	2	13

CMA: Coronary Microcalcification Activity, TRB$_{MAX}$: maximum target to background ratio

*Observations 1 and 2 were performed by Observer 1 at least 12 weeks apart in random order to prevent recall bias.

Table 3

Intraclass correlation for intraobserver and interobserver repeatability and interscan reproducibility for coronary microcalcification activity.

	Per-vessel (95% confidence interval)	Per-patient (95% confidence interval)
Intraobserver Repeatability	0.997 (0.995-0.998)	0.999 (0.998-0.999)
Interobserver Repeatability	0.994 (0.991 – 0.997)	0.995 (0.992 – 0.997)
Interscan Reproducibility	0.991 (0.986 – 0.994)	0.993 (0.992 – 0.996)

FIGURES
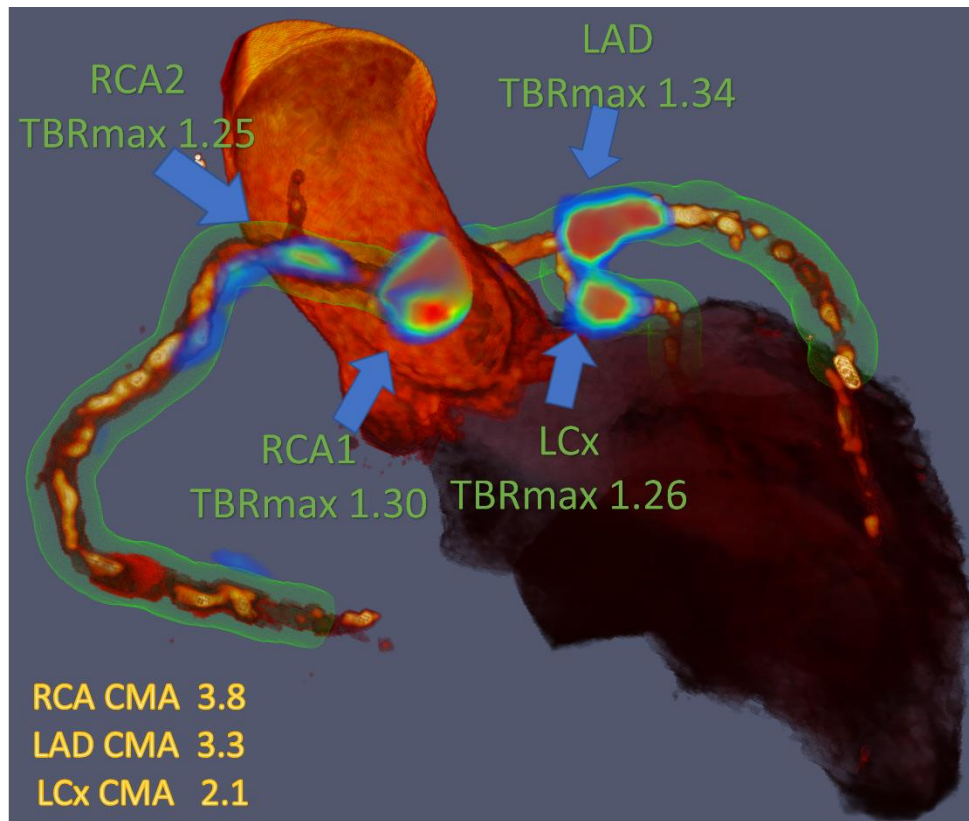
Figure 1

Three-dimensional rendering of coronary computed tomography (CT) angiography with superimposed tubular whole vessel volumes of interest (light green) employed for evaluation of ^{18}F-sodium fluoride (^{18}F-NaF) positron emission tomography (PET) uptake (blue and red). Despite the relatively low maximum tissue-to-background ratio (TBRmax) due to multiple foci of increased ^{18}F-NaF activity, the coronary microcalcification activity (CMA) in the right coronary artery (RCA) is higher than in the left anterior descending (LAD) coronary artery which presented with a higher TBRmax (LCx= Left circumflex artery).
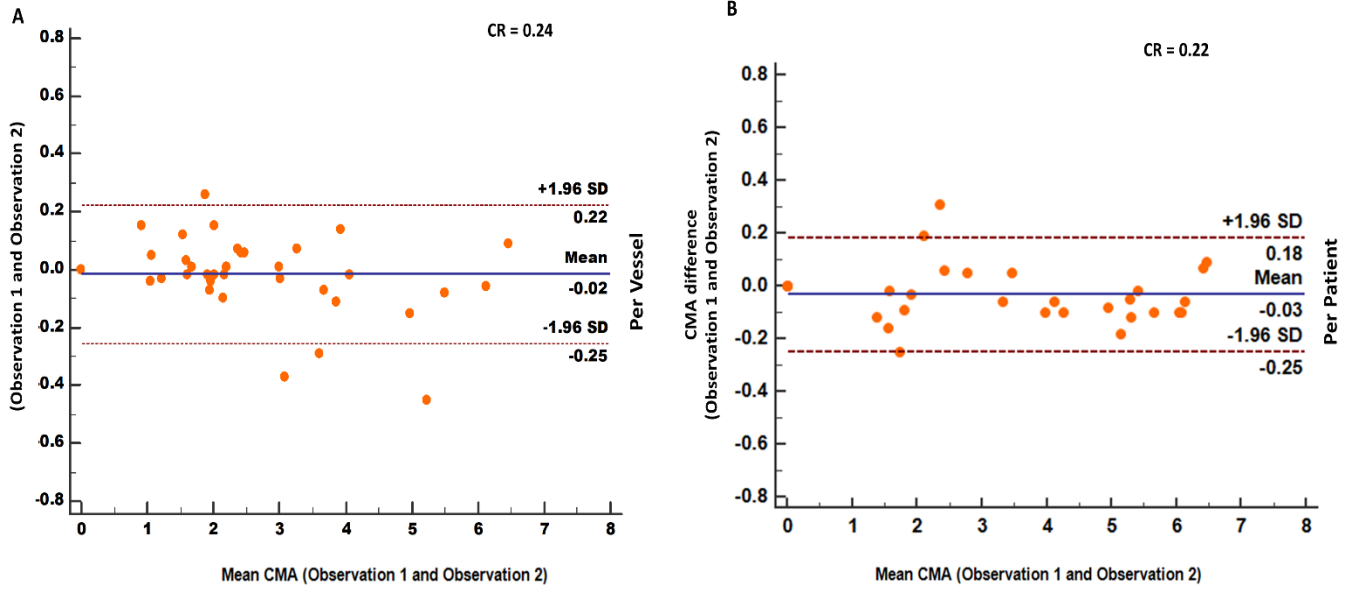
Figure 2

Intraobserver repeatability of coronary microcalcification activity at vessel (A) and

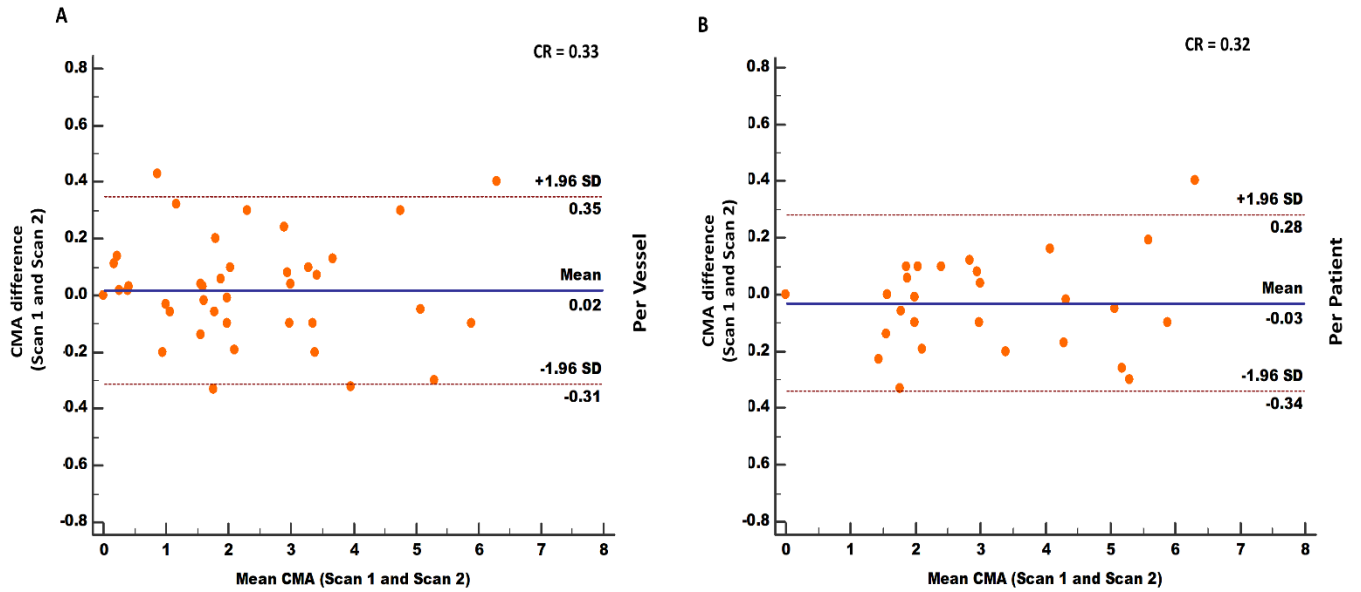patient (B) level. [CMA: coronary microcalcification activity, SD: standard deviation]
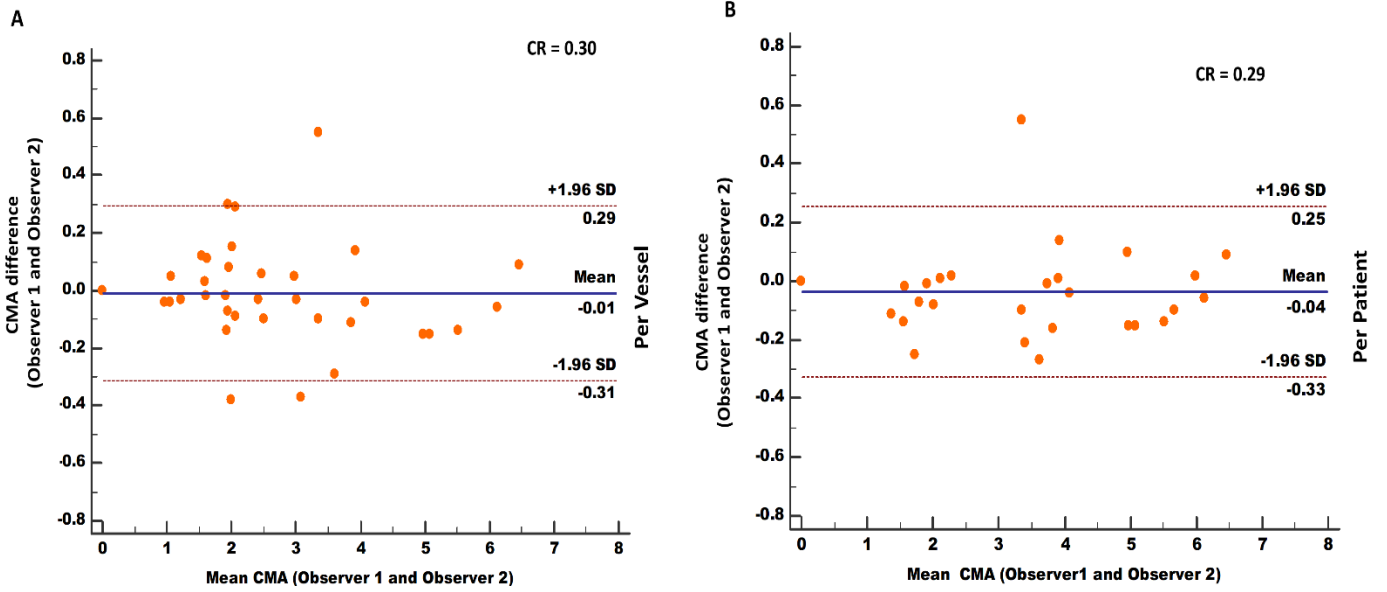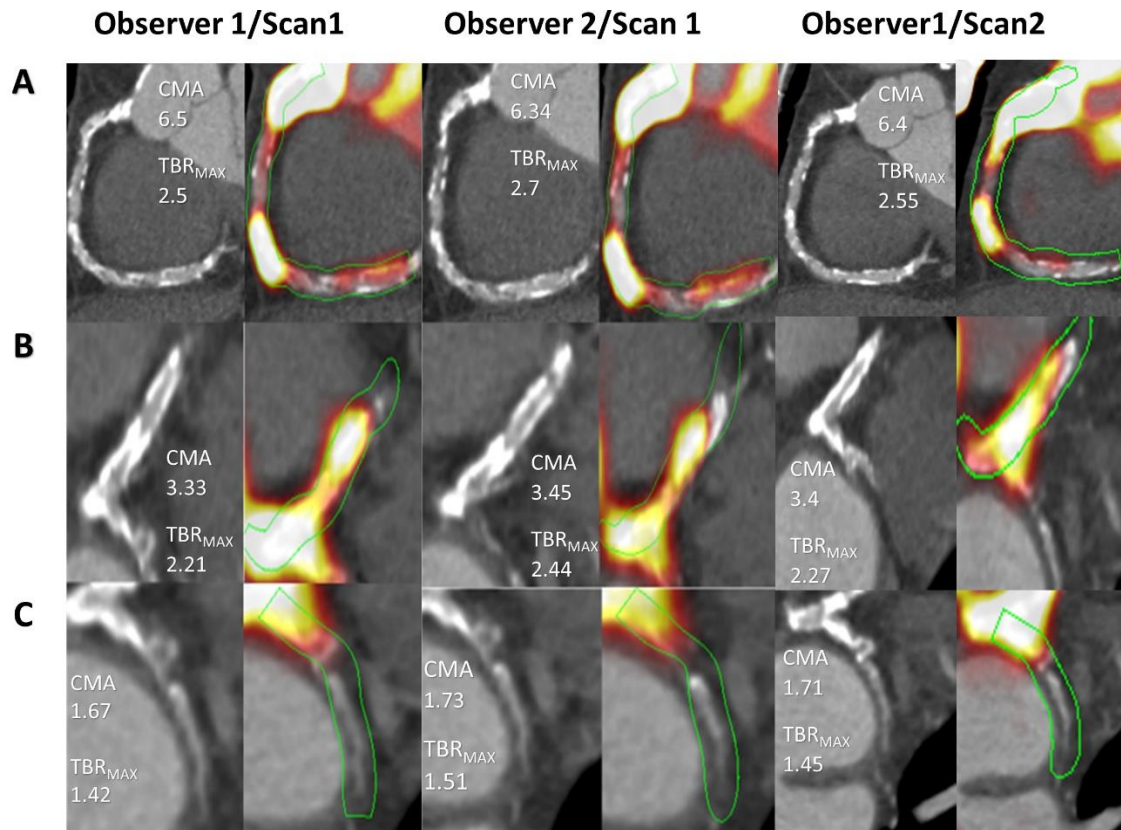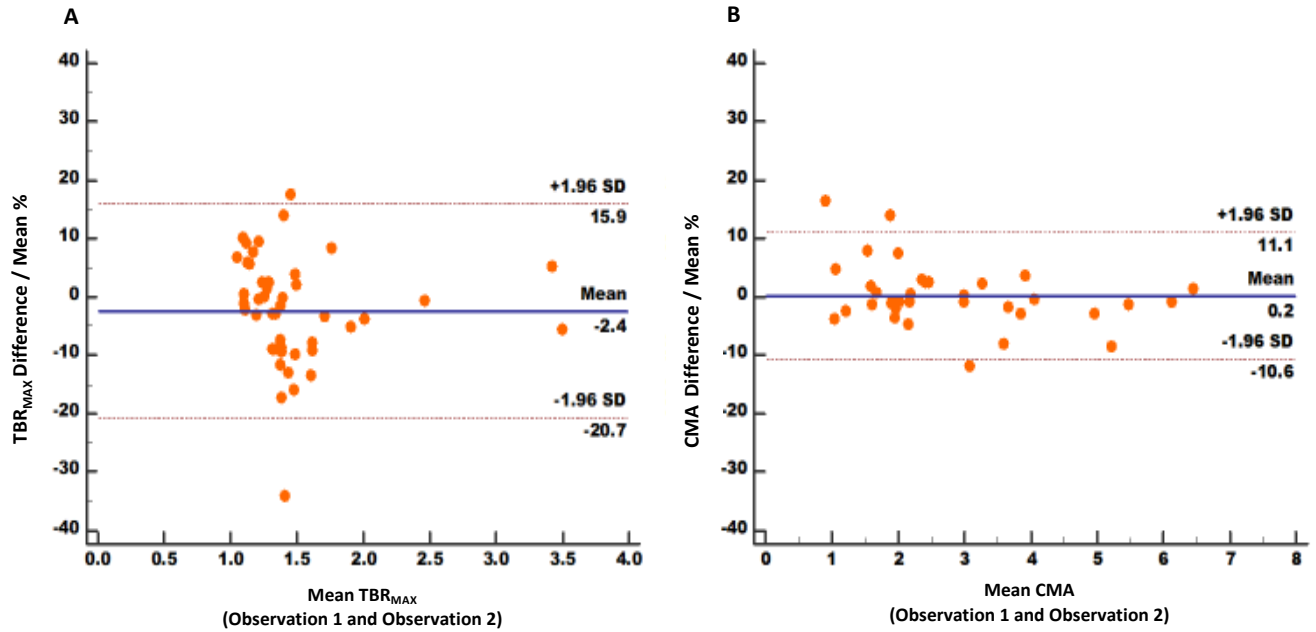
Figure 3

Interobserver repeatability of coronary microcalcification activity at vessel (A) and

patient (B) level. [CMA: coronary microcalcification activity, SD: standard deviation]
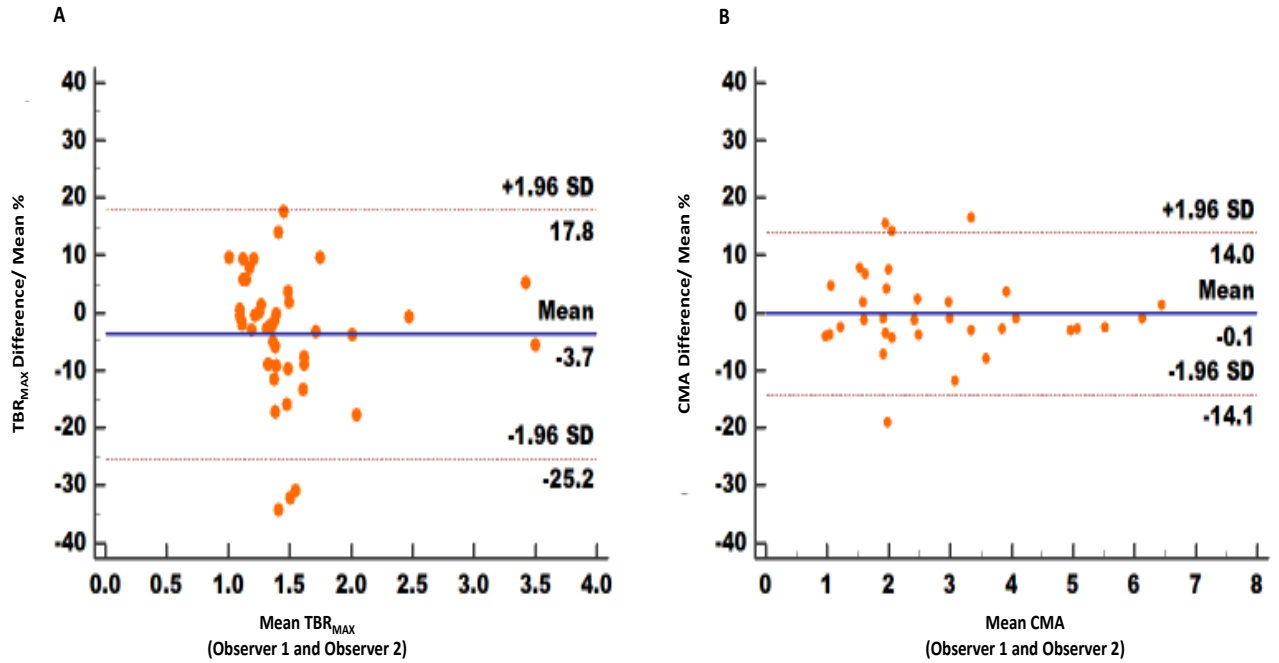
Figure 4

Interscan repeatability of coronary microcalcification activity at vessel (A) and patient (B)

level. [CMA: coronary microcalcification activity, SD: standard deviation]

Figure 5

Paired coronary tomography images (CT) and fused positron emission tomography (PET) /CT images of a representative patient with multiple lesions across the coronary tree assessed by two observers and with repeated scans. Panel (A) shows the right coronary artery (RCA) with multiple plaques across the length of the artery and respective ^{18}F-NaF PET uptake. Tubular whole vessel volumes of interest (light green) employed for evaluation of ^{18}F-NaF (PET) uptake (bright yellow to red), B) Left main stem and left anterior descending artery (LMS/LAD) with multiple plaques and ^{18}F-NaF PET uptake and C) left circumflex (LCx) with a calcified proximal plaque and uptake. [CMA: coronary microcalcification activity, TRB$_{MAX}$: maximum target to background ratio]

SUPPLEMENT

Supplement Figure 1

Intraobserver repeatability of TBRmax (A) and CMA (B) presented as % difference. [CMA:

coronary microcalcification activity, TBR$_{MAX}$: *maximum target to background ratio* SD:
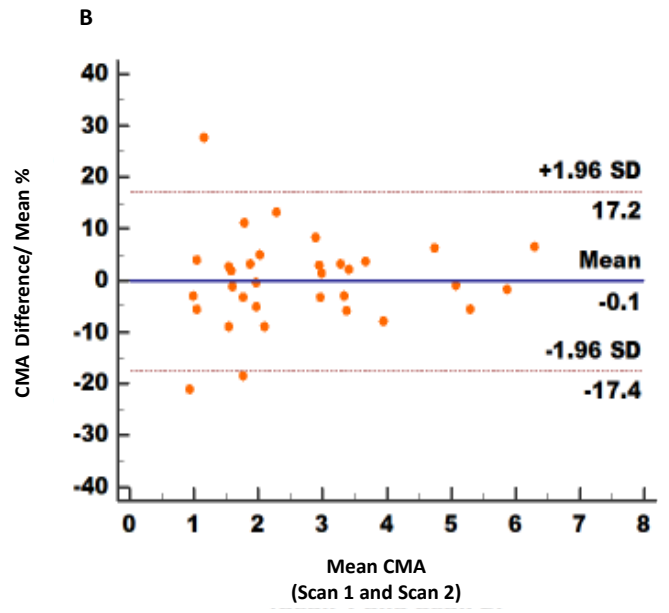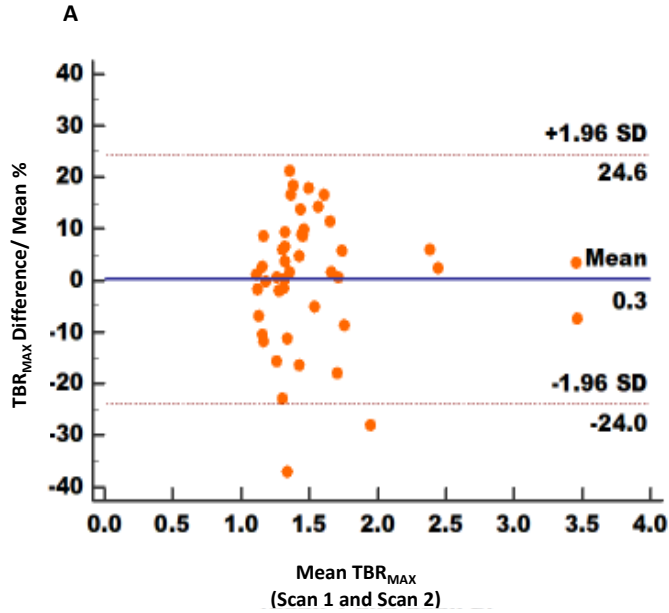
standard deviation]

Supplement Figure 2

Interobserver repeatability of TBRmax (A) and CMA (B) presented as % difference.

[CMA: coronary microcalcification activity, TBR$_{MAX}$: *maximum target to background ratio*

SD: standard deviation]

Supplement Figure 3

Interscan repeatability of TBRmax (A) and CMA (B) presented as % difference. [CMA: coronary microcalcification activity, TBR$_{MAX}$: *maximum target to background ratio* SD: standard deviation]